

Polarized J/ψ production in deep inelastic scattering at HERA

Feng Yuan

Department of Physics, Peking University, Beijing 100871, People's Republic of China

Kuang-Ta Chao

China Center of Advanced Science and Technology (World Laboratory), Beijing 100080, People's Republic of China

and Department of Physics, Peking University, Beijing 100871, People's Republic of China

Abstract

We perform a calculation on the polarization of J/ψ production in deep inelastic scattering in the HERA energy range. For the inclusive production distributions, we find that the color-singlet contributions are consistent with the experimental data in the major region of z ($z > 0.4$). Only in low z regions, there are some hints of the need of the color-octet contributions to describe the experimental data. For the polarization of J/ψ in DIS processes, we find the parameter α changes with Q^2 . Especially, at higher Q^2 , difference on α between color-singlet and color-octet contributions become more distinctive. In the two regions of lower and larger z , the polarization parameter α have different features. These properties can provide important information on the polarization mechanism for J/ψ production.

PACS number(s): 12.40.Nn, 13.85.Ni, 14.40.Gx

I. INTRODUCTION

Studies of heavy quarkonium production in high energy collisions provide important information on both perturbative and nonperturbative QCD. In the conventional picture, the heavy quarkonium production is described in the color-singlet model (CSM) [1]. In this model, it is assumed that the heavy quark pair must be produced in a color-singlet state at short distance with the same angular-momentum quantum number as the charmonium which is eventually observed. However, with the recent Tevatron data on high p_T J/ψ production, this color-singlet picture for heavy quarkonium production has become questionable. The observed cross section is larger than the theoretical prediction of the color-singlet model by a factor of about $30 \sim 50$ [2]. This is called the J/ψ (ψ') surplus problem. On the theoretical side, the naive color-singlet model has been supplanted by the nonrelativistic QCD (NRQCD) factorization formalism [3], which allows the infrared safe calculation of inclusive charmonium production and decay rates. In this approach, the production process is factorized into short and long distance parts, while the latter is associated with the nonperturbative matrix elements of four-fermion operators. So, for heavy quarkonium production, the quark-antiquark pair does not need to be in the color-singlet state in the short distance production stage, which is at the scale of $1/m_Q$ (m_Q is the heavy quark mass). At this stage, the color configuration other than the singlet is allowed for the heavy quark pair, such as color-octet. The later situation for heavy quarkonium production is called the color-octet mechanism. In this production mechanism, heavy quark-antiquark pair is produced at short distances in a color-octet state, and then hadronizes into a final state quarkonium (physical state) nonperturbatively. The color-octet terms in the gluon fragmentation to $J/\psi(\psi')$ have been considered to explain the $J/\psi(\psi')$ surplus problems discovered by CDF [4,5]. Taking the nonperturbative $\langle \mathcal{O}_8^{J/\psi}(^3S_1) \rangle$ and $\langle \mathcal{O}_8^{\psi'}(^3S_1) \rangle$ as input parameters, the CDF surplus problem for J/ψ and ψ' can be explained as the contributions of color-octet terms due to gluon fragmentation.

Apart from the NRQCD factorization approach (NRQCD FA) mentioned above, there are also other approaches for describing heavy quarkonium production in literature advocated in these years, such as the Color Evaporation Model [6], and the model of heavy quarkonium production with interactions with comoving fields [7].

Even though the color-octet mechanism has achieved some successes in describing the production and decay of heavy quarkonia, more tests of this mechanism are still needed. Recently, the photoproduction data from HERA [8,9] put a question about the color-octet predictions for the inelastic photoproduction of J/ψ [10,11] (possible solutions for this problem have been suggested in [12–15]). Most recently, the CDF collaboration have reported their preliminary measurements on the polarizations of the promptly produced charmonium and bottomonium states [16], which appear not to support the color-octet predictions that the directly produced S -wave quarkonia have transverse polarization at large p_T [17,18]. This discrepancy between the experimental results and the theoretical predictions shows that the predictions of NRQCD color-octet mechanism on the polarizations of heavy quarkonium productions may be questionable. However, the final conclusion about this problem can be achieved only if the polarizations of charmonium production in other processes are also measured and compared with theoretical predictions. In this paper, we will study the polarization of J/ψ production in deep inelastic scattering (DIS) processes at HERA collider.

The relevant photoproduction processes have been studied in [19], and the leading order color-octet J/ψ production and polarization in DIS have been studied in [20] (from $2 \rightarrow 1$ virtual photon subprocesses). These processes contribute to J/ψ production in the forward direction. In this paper, we will complete these studies by calculating the J/ψ production in DIS from the NLO color-octet processes, i.e., from the virtual photon $2 \rightarrow 2$ subprocesses. With these calculations, we can study the z distributions of J/ψ production and polarization in DIS processes at HERA, which will compensate the previous studies in the photoproduction process. Moreover, since the photon virtuality Q^2 can be large, electroproduction is a better process from which to test the color-octet mechanism and to extract the NRQCD long distance matrix elements than photoproduction. The latter process lacks any large energy scale other than the charm quark mass, and consequently, higher order perturbative corrections to leading order calculations are expected to be large. In addition, nonperturbative effects, such as higher twist corrections to the parton model, are less effectively suppressed in photoproduction than in electroproduction at large Q^2 .

The rest of the paper is organized as follows. In Sec. II, we will give the polarized cross section formula for the inelastic J/ψ production at the electron-proton collider. Here, we adopt the Weizsäcker-Williams approximation to calculate the electroproduction cross section with the photoproduction cross section. The numerical results are given in Sec. III. We will display the polarized cross sections for both the photon-proton collisions and electron-proton collisions. In Sec. IV, we give the conclusions.

II. POLARIZED CROSS SECTION FORMULAS

The polar angular distribution in $J/\psi \rightarrow l^+l^-$ decay is given by

$$\frac{d\Gamma}{d\cos\theta} \propto 1 + \alpha \cos^2\theta, \quad (1)$$

where θ is the angle between the lepton three-momentum in the J/ψ rest frame and the polarization axis. α is the polar angle asymmetry parameter,

$$\alpha = \frac{1 - 3\xi}{1 + \xi}, \quad (2)$$

where

$$\xi = \frac{d\sigma(ep \rightarrow eJ/\psi(\lambda = 0)X)}{\sum_\lambda d\sigma(ep \rightarrow eJ/\psi(\lambda)X)}. \quad (3)$$

Here λ is the helicity of the produced J/ψ . $\lambda = 0$ means J/ψ is longitudinally polarized, and $\lambda = \pm 1$ transversely polarized.

In the Born approximation, the electroproduction cross section $\sigma(ep \rightarrow eJ/\psi X)$ is related to the γ^*p cross section by

$$\frac{d\sigma(ep \rightarrow eJ/\psi X)}{dydQ^2} = \Gamma_T \sigma_T(\gamma^*p \rightarrow J/\psi X) + \Gamma_L \sigma_L(\gamma^*p \rightarrow J/\psi X). \quad (4)$$

Here $\Gamma_{T,L}$ are the flux factors of the transversely and longitudinally polarized virtual photons respectively,

$$\Gamma_T = \frac{\alpha(1 + (1 - y)^2)}{2\pi y Q^2}, \quad \Gamma_L = \frac{\alpha(1 - y)}{\pi y Q^2}, \quad (5)$$

where $y = k_{\gamma^*} \cdot P / k_e \cdot P$ is the fraction of the lepton's energy lost in the proton rest frame. In the typical kinematic region of HERA experiments, the difference between Γ_T and Γ_L is negligible. So, in practice, we can simplify the cross section formula of Eq.(4) as

$$\frac{d\sigma(ep \rightarrow eJ/\psi X)}{dydQ^2} = \Gamma_T \sigma_{tot}(\gamma^* p \rightarrow J/\psi X), \quad \text{and,} \quad \sigma_{tot} = \sigma_T + \sigma_L. \quad (6)$$

σ_T and σ_L are the cross sections for the transversely and longitudinally polarized virtual photons respectively.

There are two types of contributions to the $\gamma^* p$ cross section: the direct photoproduction and the resolved photon production. The latter contribution is through the partonic content of γ^* in the reactions. The cross section formulas (polarized and unpolarized) for the relevant partonic processes of these resolved photon production processes can be found in [19]. In the following we will calculate the polarized cross sections for the direct virtual photon ($Q^2 > 0$) processes, which include the following partonic channels,

$$\gamma^* + g \rightarrow (c\bar{c})[{}^3S_1^{(1)}, {}^3S_1^{(8)}, {}^1S_0^{(8)}, {}^3P_J^{(8)}] + g; \quad (7)$$

$$\gamma^* + q/\bar{q} \rightarrow (c\bar{c})[{}^3S_1^{(8)}, {}^1S_0^{(8)}, {}^3P_J^{(8)}] + q/\bar{q}. \quad (8)$$

In this paper, we calculate the above $2 \rightarrow 2$ subprocess contributions to production of J/ψ , and present the z distribution of the production rate. For this purpose, in the following we will not consider the $2 \rightarrow 1$ subprocess contributions, because these contributions only take place in the forward region.

To calculate these virtual photon subprocesses, we employ the helicity amplitude method. Following [21], we choose the polarization vectors for the incident and the outgoing gluons as

$$\not{e}_2^{(\pm)} = N_e [\not{p}_2 \not{p}_3 \not{q}(1 \mp \gamma_5) + \not{q} \not{p}_3 \not{p}_2(1 \pm \gamma_5)], \quad (9)$$

$$\not{e}_3^{(\pm)} = N_e [\not{p}_3 \not{q} \not{p}_2(1 \mp \gamma_5) + \not{p}_2 \not{q} \not{p}_3(1 \pm \gamma_5)]. \quad (10)$$

Where $q = p_1 + \frac{Q^2}{2p_1 \cdot p_2} p_2$, $p_1^2 = -Q^2$ and p_1 is the momentum for the incident photon. p_2 , p_3 and e_2 , e_3 are the momenta and the polarization vectors for the incident gluon and outgoing gluon respectively. The normalization factor N_e is

$$N_e = \frac{1}{\sqrt{2(Q^2 M^2 + \hat{s}\hat{u})\hat{t}}}, \quad (11)$$

where M is the mass of J/ψ . The Mandelstam invariants \hat{s} , \hat{t} , \hat{u} are defined as

$$\hat{s} = (p_1 + p_2)^2, \quad \hat{t} = (p_2 - p_3)^2, \quad \hat{u} = (p_1 - p_3)^2, \quad (12)$$

and they satisfy the relation

$$\hat{s} + \hat{t} + \hat{u} = M^2 - Q^2.$$

For the transversely polarized photons, we have the following projection operator,

$$P_{\mu\nu}^{\gamma T} = \epsilon_\mu^*(T)\epsilon_\nu(T) = -g_{\mu\nu} + \frac{p_{2\mu}q_\mu + p_{2\nu}q_\nu}{p_2 \cdot q}, \quad (13)$$

and for the longitudinally polarized photons, we have

$$P_{\mu\nu}^{\gamma L} = \epsilon_\mu^*(L)\epsilon_\nu(L) = \frac{1}{Q^2}(p_{1\mu} + \frac{Q^2}{p_1 \cdot p_2}p_{2\mu})(p_{1\nu} + \frac{Q^2}{p_1 \cdot p_2}p_{2\nu}). \quad (14)$$

Providing with the above defined polarized vectors and polarized projection tensors, we can calculate the amplitude squared for the partonic processes with the definite helicities of the incident and the outgoing partons. After summing up the helicities and colors, we express the amplitude squared as the following form

$$\mathcal{M}(ij \rightarrow J/\psi^{(\lambda)} X) = \sum_n F_{ij}^{(\lambda)}[n] \langle \mathcal{O}_n^{J/\psi} \rangle, \quad (15)$$

where the short-distance coefficients F can be written as

$$\begin{aligned} F_{ij}^{(\lambda)}[n] = & A_{ij}[n][\epsilon^*(\lambda) \cdot \epsilon(\lambda)] \\ & + B_{ij}[n][\epsilon^*(\lambda) \cdot p_1 \epsilon(\lambda) \cdot p_1] \\ & + C_{ij}[n][\epsilon^*(\lambda) \cdot p_2 \epsilon(\lambda) \cdot p_2] \\ & + D_{ij}[n][\epsilon^*(\lambda) \cdot p_1][\epsilon(\lambda) \cdot p_2]. \end{aligned} \quad (16)$$

Here n denote the intermediated states, which include ${}^3S_1^{(1)}$, ${}^3S_1^{(8)}$, ${}^1S_0^{(8)}$, ${}^3P_J^{(8)}$. The A , B , C , D functions for different partonic processes are listed in the Appendix.

For convenience, we consider the J/ψ polarization in the *target* frame. In this frame, the covariant expression for the polarization vector of J/ψ with helicity $\lambda = 0$ reads [19]

$$\epsilon_\mu^{(\lambda=0)}(p_\psi) = \frac{1}{M}p_{\psi\mu} - \frac{M}{p_\psi \cdot p_2}p_{2\mu}. \quad (17)$$

With this equation and Eqs.(15-16), we can calculate the polarized cross sections, and obtain the polar angle asymmetry parameter α in Eq.(2).

We have checked that our cross section formulas can reproduce the photoproduction cross section formulas [19] at $Q^2 = 0$, and that the unpolarized cross section for the color-singlet process is consistent with that of [22].

III. NUMERICAL RESULTS

The production rate of J/ψ and its polarization parameter α depend on the sizes of the NRQCD long distance matrix elements, including the color-singlet matrix elements and the color-octet matrix elements. We choose these matrix elements as

$$\langle \mathcal{O}_1^\psi({}^3S_1) \rangle = 1.16 \text{GeV}^3, \quad (18)$$

$$\langle \mathcal{O}_8^\psi({}^3S_1) \rangle = 1.06 \times 10^{-2} \text{GeV}^3, \quad (19)$$

$$\langle \mathcal{O}_8^\psi({}^1S_0) \rangle = 3.0 \times 10^{-2} \text{GeV}^3, \quad (20)$$

$$\langle \mathcal{O}_8^\psi({}^3P_0) \rangle / m_c^2 = 1.0 \times 10^{-2} \text{GeV}^3, \quad (21)$$

$$\langle \mathcal{O}_8^\psi({}^3P_J) \rangle = (2J+1) \langle \mathcal{O}_8^\psi({}^3P_0) \rangle. \quad (22)$$

The color-singlet matrix element $\langle \mathcal{O}_1^\psi(^3S_1) \rangle$ can be related to the $c\bar{c}$ wave function at the origin, and can be taken from the leptonic decay width of J/ψ . The last equation comes from the approximation of heavy quark spin symmetry of NRQCD. The value of the color-octet matrix element $\langle \mathcal{O}_8^\psi(^3S_1) \rangle$ is taken from a fit to the large p_T J/ψ production at the Tevatron [25]. This matrix element is not important to J/ψ photoproduction both for the production rate and the polarization parameter α . On the other hand, the other two color-octet matrix elements, $\langle \mathcal{O}_8^\psi(^1S_0) \rangle$ and $\langle \mathcal{O}_8^\psi(^3P_0) \rangle$, are known to be very important in the inelastic J/ψ photoproduction [10,19]. However, their values are not well determined from the present experimental data on J/ψ productions. Here, we just follow Ref. [19] and take their values tentatively as listed above (which are also consistent with the naive NRQCD velocity scaling rules) to see what are their contributions to the cross section and the polarization α of J/ψ production in DIS at HERA. For the numerical evaluation, we choose $m_c = 1.5 \text{ GeV}$, and set the renormalization scale and the factorization scale both equal to $\mu^2 = (2m_c)^2 + Q^2$. For the parton distribution functions of the proton, we use the Glück-Reya-Vogt (GRV) LO parameterization [24].

We first display the z distribution of the inelastic J/ψ production rate in DIS region at HERA, comparing the theoretical predictions with the ZEUS data [9]¹. The kinematic region is $2\text{GeV}^2 < Q^2 < 80\text{GeV}^2$ and $40\text{GeV} < W_{\gamma^*p} < 180\text{GeV}$. In Fig. 1, the dotted line is for the color-singlet contribution, the dotted-dashed line for the direct virtual photon contributions from the color-octet processes, and the dashed line for the resolved virtual photon contributions from the color-octet processes. For the above two components of the color-octet contributions, we choose the color-octet matrix elements of $\langle \mathcal{O}_8^\psi(^1S_0) \rangle$ and $\langle \mathcal{O}_8^\psi(^3P_0) \rangle$ as $\langle \mathcal{O}_8^\psi(^1S_0) \rangle = \langle \mathcal{O}_8^\psi(^3P_0) \rangle / m_c^2 = 0.008\text{GeV}^3$. And the solid lines correspond to the NRQCD FA predictions (including the color-singlet contributions and the color-octet contributions) for the two choices of the color-octet matrix elements: (I) for the lower solid line,

$$\begin{aligned} \langle \mathcal{O}_8^\psi(^1S_0) \rangle &= 3.0 \times 10^{-2}\text{GeV}^3, \\ \langle \mathcal{O}_8^\psi(^3P_0) \rangle / m_c^2 &= 0; \end{aligned} \quad (23)$$

(II) for the upper solid line,

$$\begin{aligned} \langle \mathcal{O}_8^\psi(^1S_0) \rangle &= 0, \\ \langle \mathcal{O}_8^\psi(^3P_0) \rangle / m_c^2 &= 1.0 \times 10^{-2}\text{GeV}^3. \end{aligned} \quad (24)$$

From this figure, we can also see that the rapid increase of the color-octet predictions at large z is not supported by the experimental data. This is similar to the case of the J/ψ photoproduction ($Q^2 = 0$), and may indicate that at large z the calculations of the color-octet processes are also unreliable due to higher order v^2 contributions [14]. On the other hand, we find that the color-singlet contributions are consistent with the experimental data in the

¹These data have also been compared with the theoretical predictions in [26]. However, this study is not relevant to the electroproduction process because the author made an approximation for the cross sections of virtual photon processes by using those of real photon processes.

major region of z . However, as indicated by the color-singlet photoproduction processes calculations [11,19], the color-singlet cross sections have large theoretical uncertainties due to input parameters such as the normalization and factorization scales and the charm quark mass. In this context, it is difficult to immediately conclude that the experimental data are just saturated by the color-singlet contributions and there is no more space for the color-octet contributions. Especially, in the lower z region the experimental data lie above the color-singlet contributions, where the dominant contributions come from the color-octet channels in the resolved photon processes. (The color-singlet contributions in the resolved photon processes is much smaller than the color-octet contributions, and is not presented in Fig. 1). This may be viewed as a hint of the need of the color-octet contributions in describing the experimental data on J/ψ photoproduction in the lower z region.

We now turn to study the angular distributions of J/ψ productions. Since the decay angular distribution parameter α is normalized, its dependence on parameters that affect the absolute normalization of the production cross sections, such as the charm quark mass, the strong coupling constant, the renormalization and factorization scales and the parton distribution functions, cancels to a large extent and does not constitute a significant uncertainty. That is to say, in some sense, the polarization parameter as a tool for testing production mechanism is more efficient than the absolute production rate. In Fig. 2, we first display the polarization parameter α as a function of z for the γ^*p processes, where the c.m. energy of γ^*p system is set to be $W_{\gamma^*p} = 100\text{GeV}$. Here in this figure we do not include the resolved photon processes contributions. The solid lines are for the CSM predictions, and the other two lines are for the NRQCD FA (including both the color-singlet and color-octet contributions) corresponding to the two choices of the color-octet matrix elements: the dashed lines for the choice of Eq. (23) and the dotted-dashed lines for the choice of Eq. (24). In order to see the Q^2 dependence of the polarization, we choose four typical values for Q^2 : 0, 4, 10, 40GeV^2 . From these plots, we can see that the polarization parameter α in large z region change from positive values to negative values as Q^2 increases. This means that in large z region J/ψ production will be dominantly longitudinally polarized at high Q^2 . Especially, the polarization parameter α for CSM predictions are more sensitive to Q^2 than those for the NRQCD FA predictions. At high Q^2 , e.g., $Q^2 = 40\text{GeV}^2$, the difference on α between CSM and NRQCD FA can be distinguished for large z J/ψ production (see Fig. 2). In this case, the CSM prediction approaches to $\alpha = -0.7$ while the NRQCD FA predictions are both above -0.4 for the two choices of the color-octet matrix elements (Eqs. (23) and (24)). In addition, we note that if $^1S_0^{(8)}$ channel dominates J/ψ production the polarization parameter α will be close to zero because in this case the produced J/ψ are unpolarized, which can also be seen from Fig. 2.

In Fig. 3, we show the parameter α as a function of z for ep collisions at HERA (including the resolved photon contributions). As in Fig. 2, we choose two typical regions for Q^2 : (a) $2\text{GeV}^2 < Q^2 < 80\text{GeV}^2$, and (b) $10\text{GeV}^2 < Q^2 < 80\text{GeV}^2$. From this figure, we also find that the J/ψ polarization changes with Q^2 . Especially, at higher Q^2 , the difference on α between CSM predictions and NRQCD FA predictions become more distinctive. In the two regions of lower and larger z , the polarization parameter α have different features. In the lower z region, the NRQCD FA predicts J/ψ being transversely polarized for the octet matrix elements choice of Eq. (24), while the CSM predicts J/ψ to be only slightly polarized (almost compatible with unpolarized). We note that in this region, the dominant

contributions in the NRQCD FA come from the color-octet resolved photon processes (see Fig. 1), which have the similar properties as they have for J/ψ hadroproduction, contributing to J/ψ transverse polarization [17]. In Fig. 3, for larger z , on the other hand we find that the CSM predicts J/ψ being more polarized, which is however longitudinal. The NRQCD FA predicts J/ψ less polarized (also longitudinally if ${}^3P_J^{(8)}$ dominates). Again, we note if J/ψ production is dominated by ${}^1S_0^{(8)}$ channel, it will be unpolarized as that for γ^*p processes.

In the above analyzes, we present the NRQCD FA predictions of the polarization parameters α by using the color-octet matrix elements as in Eqs. (23) and (24). However, there are other sets of parameterizations for the two color-octet matrix elements $\langle \mathcal{O}_8^\psi({}^1S_0) \rangle$ and $\langle \mathcal{O}_8^\psi({}^3P_0) \rangle$ in the literature [12,13]. With these rather small values for the two color-octet matrix elements [12,13], the above predictions of α in the NRQCD FA will be changed. For example, if we follow the values obtained in [13], the two equations of (23) and (24) will be changed to

$$\begin{aligned} \langle \mathcal{O}_8^\psi({}^1S_0) \rangle &= 5.72 \times 10^{-3} \text{GeV}^3, \\ \langle \mathcal{O}_8^\psi({}^3P_0) \rangle / m_c^2 &= 0; \end{aligned} \quad (25)$$

for case (I), and

$$\begin{aligned} \langle \mathcal{O}_8^\psi({}^1S_0) \rangle &= 0, \\ \langle \mathcal{O}_8^\psi({}^3P_0) \rangle / m_c^2 &= 1.62 \times 10^{-3} \text{GeV}^3, \end{aligned} \quad (26)$$

for case (II). If we use the above values for the matrix elements of $\langle \mathcal{O}_8^\psi({}^1S_0) \rangle$ and $\langle \mathcal{O}_8^\psi({}^3P_0) \rangle$, the difference of the polarization parameter α between the CSM and the NRQCD FA will be reduced, because with these rather small values for the color-octet matrix elements the color-octet contributions to J/ψ production are much less important than those with parameterizations of Eqs. (23) and (24). This influence is presented in Fig. 4, where we show the same plot as in Fig. 3 but with the new parameterizations of the color-octet matrix elements as in Eqs. (25) and (26). From this figure, we can see that the difference between these two approaches is reduced, though in some regions there are still some differences.

IV. CONCLUSIONS

In this paper, we have calculated J/ψ production and polarization in DIS at ep colliders in the energy region relevant to HERA. Compensating for the previous color-octet leading order calculations, we have calculated the cross sections for the γ^*p $2 \rightarrow 2$ subprocesses which are needed for theoretical evaluations of the z distributions of the production rate and the polarization parameter α . For the inclusive production distributions, we find that the color-singlet contributions are consistent with the experimental data in the major region of z ($z > 0.4$). Only in the low z regions, there are some hints of the need of the color-octet contributions to describe the experimental data.

For the polarization of J/ψ in DIS processes, we find the parameter α changes with Q^2 . Especially, at higher Q^2 , difference on α between the CSM and the NRQCD FA become more distinctive. In the two regions of lower and larger z , the polarization parameter α have different features. In the lower z region, the NRQCD FA predicts J/ψ being transversely

polarized if the ${}^3P_J^{(8)}$ channel dominates, while the CSM J/ψ being almost unpolarized. On the other hand, in the larger z region the CSM predicts J/ψ being longitudinally polarized, while the NRQCD FA predicts J/ψ being unpolarized if the ${}^1S_0^{(8)}$ channel dominates. In conclusion, the polarization of J/ψ in DIS processes at ep colliders will give another independent test for the production mechanism and help to clarify the present problem concerning the disagreement of the theoretical predictions with the experimental data on polarization in hadroproduction processes at the Tevatron.

ACKNOWLEDGMENTS

We thank M. Krämer for sending us their amplitude codes of Ref. [19]. This work was supported in part by the National Natural Science Foundation of China, the State Education Commission of China, and the State Commission of Science and Technology of China.

APPENDIX:

In this appendix, we list the A , B , C , D functions of Eq.(16) in the short distance coefficients of the amplitude squared for every partonic processes². For convenience, we define the following variables relevant to the Mandelstam invariants (\hat{s} , \hat{t} , and \hat{u}): $s = 2p_1 \cdot p_2 = \hat{s} + Q^2$, $u = -2p_1 \cdot p_3 = \hat{u} + Q^2$, $t = 2p_2 \cdot p_3 = \hat{t}$
 $\gamma_T^* + g \rightarrow c\bar{c}({}^3S_1, \underline{1}) + g$:

$$F = \frac{16M(4\pi)^3\alpha\alpha_s^2e_c^2\langle\mathcal{O}_1^\psi({}^3S_1)\rangle}{27(s+t)^2(s+u)^2(t+u)^2s^2}, \quad (\text{A1})$$

$$a = s^2[stu(s+t+u) - (st+tu+su)^2] - 2Q^2(Q^2t^2 + stu)(s^2 + t^2), \quad (\text{A2})$$

$$b = 2s^2[2Q^2t^2 - (s^2 + t^2)(s+t+u)], \quad (\text{A3})$$

$$c = 2[4Q^6t^2 + 4Q^4t(su - t^2 - tu) + 2Q^2s(st^2 + su^2 - s^2t - t^2u - tu^2) - s^2(s+t+u)(s^2 + u^2)], \quad (\text{A4})$$

$$d = 4s[Q^2t(2Q^2t - s^2 - t^2 - tu) - s^3(s+t+u)]. \quad (\text{A5})$$

²It is easy to check that our A , B , C , D functions reproduce the results of Ref. [19] in the photoproduction limit. Using these expressions, one can also get the unpolarized cross sections for different subprocesses, which were reproduced by the authors of [27] for the $\gamma_T^* + g(q)$ processes. However, there is a factor of 2 difference from theirs for the $\gamma_L^* + g(q)$ processes except the $\gamma_L^* + g \rightarrow c\bar{c}({}^1S_0, \underline{8}) + g$ process. We note, however, that our unpolarized cross sections for the color-singlet processes $\gamma_{T/L}^* + g \rightarrow c\bar{c}({}^3S_1, \underline{1}) + g$ are consistent with those of [22]. The computer code for these expressions can be obtained by requiring to ktchao@pku.edu.cn.

$\gamma_L^* + g \rightarrow c\bar{c}(^3S_1, \underline{1}) + g$: F is the same as Eq.(A1) and $b = 0$,

$$a = -2Q^2t^3(Q^2t + su), \quad (\text{A6})$$

$$c = 4Q^2[2Q^2(Q^2t^2 + stu - t^3 - t^2u) + su(s - t)(t + u)], \quad (\text{A7})$$

$$d = 4Q^2st[su + t(Q^2 - M^2)]. \quad (\text{A8})$$

$\gamma_{T,L}^* + g \rightarrow c\bar{c}(^3S_1, \underline{8}) + g$: the functions are the same as the above $\gamma_{T,L}^* + g \rightarrow c\bar{c}(^3S_1, \underline{1}) + g$ processes but multiplied by the factor

$$\frac{15}{8} \frac{\langle \mathcal{O}_8^\psi(^3S_1) \rangle}{\langle \mathcal{O}_1^\psi(^3S_1) \rangle}. \quad (\text{A9})$$

$\gamma_T^* + g \rightarrow c\bar{c}(^1S_0, \underline{8}) + g$:

$$Fa = \frac{-(4\pi)^3 \alpha \alpha_s^2 e_c^2 \langle \mathcal{O}_8^\psi(^1S_0) \rangle}{Ms^2 t(s+t)^2(s+u)^2(t+u)^2} (Q^2t + su)[4Q^4t^2u^2 + 4Q^2stu(t^2 + u^2 + tu + ts + us) + s^2(s^4 + t^4 + u^4 + (s+t+u)^4)]. \quad (\text{A10})$$

$\gamma_L^* + g \rightarrow c\bar{c}(^1S_0, \underline{8}) + g$:

$$Fa = \frac{-4(4\pi)^3 \alpha \alpha_s^2 e_c^2 \langle \mathcal{O}_8^\psi(^1S_0) \rangle}{Ms^2(s+t)^2(s+u)^2(t+u)^2} Q^2[2Q^4t^2u^2 + 2Q^2stu(t^2 + 2u^2 + tu + ts + us) + s^2((t^2 + u^2)(t^2 + 2tu + 2u^2) + 2s(t+u)(t^2 + tu + u^2) + s^2(t+u)^2)]. \quad (\text{A11})$$

$\gamma_T^* + g \rightarrow c\bar{c}(^3P_J, \underline{8}) + g$:

$$F = \frac{24(4\pi)^3 \alpha \alpha_s^2 e_c^2 \langle \mathcal{O}_8^\psi(^3P_0) \rangle}{M^3 s^2 t^2 (s+t)^3 (s+u)^4 (t+u)^3}, \quad (\text{A12})$$

$$\begin{aligned} a = & -t[-8Q^8t^2(s^2 + t^2)(s^2 - tu)(st - u^2) + 2Q^6t(s^3(5t^5 + 3t^4u - 8t^3u^2 + 16t^2u^3 + 2u^5) \\ & - s^2t(t^5 + 9t^4u + 4t^3u^2 - 10tu^4 - 2u^5) + s^4(7t^4 - 7t^3u + 4t^2u^2 - 2tu^3 + 4u^4) - st^2u(6t^4 \\ & + 11t^3u - t^2u^2 + 5tu^3 - u^4) + s^5(7t^3 + 9t^2u - 2tu^2 + 8u^3) + 4s^6(2t^2 + u^2) + 2(t+u)s^7 \\ & - t^6u^2 + 3t^5u^3 + 5t^4u^4 + t^3u^5) - 2Q^4(s^4(5t^6 + 7t^5u - 5t^4u^2 + 6t^3u^3 - 8t^2u^4 + 5tu^5 - 2u^6) \\ & - s^2t^2(t^6 + 8t^5u + 12t^4u^2 + 5t^3u^3 + 10t^2u^4 - 5tu^5 - u^6) + s^5(9t^5 + 2t^4u + 4t^3u^2 - 5t^2u^3 \\ & + 8tu^4 - 4u^5) + s^3tu(t^5 + 7t^4u + t^3u^2 + 7t^2u^3 - tu^4 + u^5) + s^6(9t^4 + 7t^3u - 2t^2u^2 + 8tu^3 \\ & - 6u^4) - (t+u)st^3u(2t^4 + 8t^3u + 5t^2u^2 + 9tu^3 + 2u^4) + s^7(9t^3 + 4t^2u + 5tu^2 - 4u^3) \\ & + s^8(3t - 2u)(t+u) - t^8u^2 - 2t^7u^3 - t^6u^4) + Q^2s(s^3(3t^7 + 29t^6u + 56t^5u^2 + 34t^4u^3 \\ & + 26t^3u^4 + 6t^2u^5 - 6tu^6 - 6u^7) + s^4(11t^6 + 30t^5u + 6t^4u^2 - 8t^3u^3 - 22t^2u^4 - 13tu^5 - 18u^6) \\ & + s^2tu(8t^6 + 45t^5u + 76t^4u^2 + 60t^3u^3 + 49t^2u^4 + 11tu^5 - u^6) + 2s^5(7t^5 + 5t^4u - 3t^3u^2 \\ & - 14t^2u^3 - 11tu^4 - 14u^5) + s^6(14t^4 + 13t^3u - 8t^2u^2 - 19tu^3 - 28u^4) + st^2u^2(t+u)(7t^4 \\ & + 24t^3u + 18t^2u^2 + 18tu^3 + 5u^4) + s^7(11t^3 + t^2u - 12tu^2 - 18u^3) + 2(t+u)^2t^5u^3 \\ & + 3(t+u)(t-2u)s^8) + s^4u^2(10t^6 + 48t^5u + 80t^4u^2 + 67t^3u^3 + 45t^2u^4 + 19tu^5 + 3u^6) \\ & + s^5u(6t^6 + 48t^5u + 108t^4u^2 + 114t^3u^3 + 85t^2u^4 + 45tu^5 + 12u^6) + s^6(t^6 + 22t^5u + 80t^4u^2 \\ & + 114t^3u^3 + 102t^2u^4 + 61tu^5 + 22u^6) + s^7(2t^5 + 27t^4u + 67t^3u^2 + 85t^2u^3 + 61tu^4 + 26u^5) \\ & + s^3tu^3(t+u)(6t^4 + 16t^3u + 11t^2u^2 + 8tu^3 + 3u^4) + s^8(t^4 + 19t^3u + 45t^2u^2 + 45tu^3 \\ & + 22u^4) + s^9u(11t^2 + 19tu + 12u^2) + s^2t^4u^4(t+u)^2 + s^{10}u^3(t+u)] \end{aligned} \quad (\text{A13})$$

$$\begin{aligned}
b = & 2[4Q^4t^2(st - u^2)(2s^4t - s^4u - 2s^3tu - s^3u^2 - 4s^2t^2u - 2s^2tu^2 - st^3u - 2st^2u^2 - t^3u^2) \\
& - 2Q^2st(s^3(2t^5 - 2t^4u - 13t^3u^2 - 16t^2u^3 - 5tu^4 - 2u^5) + s^2t(t^5 - t^4u - 13t^3u^2 - 12t^2u^3 \\
& - 10tu^4 - 2u^5) + s^4(8t^4 + 9t^3u - 8t^2u^2 - 3tu^3 - 4u^4) + s^5(11t^3 + 6t^2u + tu^2 - 4u^3) \\
& + st^2u(t + u)(t^3 - 4t^2u - tu^2 - 2u^3) + s^6(6t^2 + 5tu - 2u^2) - 2t^3u^3(t^2 + tu + u^2) + 2s^7t) \\
& - s^4t(t^6 + 10t^5u + 25t^4u^2 + 23t^3u^3 + 25t^2u^4 + 16tu^5 + 4u^6) - s^5t(t^5 + 10t^4u + 21t^3u^2 \\
& + 19t^2u^3 + 17tu^4 + 12u^5) + s^7(4t^4 - t^3u + 2t^2u^2 - 3tu^3 + 2u^4) - s^3t^2u(t + u)(2t^4 + 9t^3u \\
& + 3t^2u^2 + 8tu^3 + 4u^4) + s^6t(2t^4 - 5t^3u - 10t^2u^2 - 3tu^3 - 10u^4) \\
& + s^8(3t^3 + t^2u - 2tu^2 + 2u^3) - s^2t^5u^2(t^2 + 2tu - u^2) + s^9t(t - u)]M^2
\end{aligned} \tag{A14}$$

$$\begin{aligned}
c = & -2[-16Q^8t^3(s^2 - tu)(st - u^2) - 4Q^6t^2(s^2(t^4 + 3t^3u + 4tu^3 - 4u^4) + su(2t - u)(3t^3 \\
& + 5t^2u + 2tu^2 + 2u^3) - s^3(t + 2u)(5t^2 - tu + 4u^2) - 4s^4(t^2 + u^2) - 2(t + u)s^5 + t^4u^2 \\
& - 5t^3u^3 - 6t^2u^4 - 2tu^5) + 4Q^4t(s^2(t^6 + 8t^5u + 9t^4u^2 + 8t^3u^3 + 10t^2u^4 + tu^5 + 2u^6) \\
& + stu(2t^5 + 10t^4u + 11t^3u^2 + 13t^2u^3 + 7tu^4 + u^5) + s^3u(t^4 + t^3u + 6t^2u^2 - 3tu^3 + 4u^4) \\
& - s^4(t^4 - t^3u - 8t^2u^2 + 2tu^3 - 6u^4) - s^5(2t^3 - 3t^2u + 2tu^2 - 4u^3) + s^6(t^2 + tu + 2u^2) \\
& + t^6u^2 + 2t^5u^3 - t^3u^5 - t^2u^6) + 2Q^2st(su^3(11t^4 + 10t^3u + 6t^2u^2 - tu^3 - 2u^4) + s^2u^2(11t^4 \\
& + 9t^3u + t^2u^2 + 3tu^3 - 5u^4) + s^4(5t^4 + 5t^3u - 12t^2u^2 - 6tu^3 - 18u^4) + s^3u(5t^4 - 16t^2u^2 \\
& - 5tu^3 - 12u^4) + 2s^5(2t^3 - t^2u - tu^2 - 7u^3) + s^6(3t^2 + 3tu - 5u^2) - 2tu^5(2t^2 + 2tu + u^2) \\
& + 2s^7t) + s^5u(2t^5 + 18t^4u + 6t^3u^2 - 15t^2u^3 - tu^4 - 2u^5) + s^6u(13t^4 + 12t^3u - 15t^2u^2 \\
& - 6tu^3 - 6u^4) + s^4tu^2(4t^4 + 18t^3u + 12t^2u^2 - tu^3 + 3u^4) + s^3tu^3(2t^4 + 13t^3u + 7t^2u^2 \\
& + tu^3 + u^4) + s^7(t - u)(t^3 + 8t^2u + 7tu^2 + 6u^3) - s^8(2t^2 + tu - 2u^2)(t - u) \\
& + s^2t^2u^5(t^2 - 2tu - u^2) - (t - u)s^9t]M^2
\end{aligned} \tag{A15}$$

$$\begin{aligned}
d = & -2[-8Q^6t^3(st - u^2)(2s^3 - s^2u - 3stu - su^2 - tu^2) + 4Q^4t^2(stu^2(t^3 + 2t^2u + 6tu^2 + u^3) \\
& + s^4t(5t^2 + 7tu + 4u^2) - s^3u(t + u)(2t^2 + 3tu + 3u^2) - s^2u(2t^2 + u^2)(t^2 + 4tu + u^2) \\
& + s^5(5t + 2u)(t + u) + 2s^6(2t + u) + t^4u^3 + t^3u^4 + 2t^2u^5) + 2Q^2st(s^2(2t^6 + 14t^5u + 37t^4u^2 \\
& + 42t^3u^3 + 37t^2u^4 + 18tu^5 + 2u^6) + stu(4t^5 + 15t^4u + 31t^3u^2 + 33t^2u^3 + 25tu^4 + 6u^5) \\
& + s^3(3t^5 + 21t^4u + 30t^3u^2 + 22t^2u^3 + 19tu^4 + 3u^5) + s^4(7t^4 + 18t^3u + 8t^2u^2 + 14tu^3 - u^4) \\
& + s^5(7t^3 + 9t^2u + 11tu^2 - 3u^3) + s^6(7t^2 + 12tu - u^2) + 2t^2u^2(t^2 + tu + 2u^2)(t^2 + tu + u^2) \\
& + 4s^7t) - s^6(t^5 - 7t^4u + 3t^3u^2 + 29t^2u^3 + 6tu^4 + 4u^5) - s^7(3t^4 + 4t^3u + 19t^2u^2 + 10tu^3 \\
& + 8u^4) + s^3t^2u^2(t^4 + 4t^3u + 19t^2u^2 + 18tu^3 + 6u^4) - s^5t(t + u)(t^4 - t^3u - 15t^2u^2 + 9tu^3 \\
& - 8u^4) - (t + u)s^4tu(t^4 - 5t^3u - 15t^2u^2 - 12tu^3 - 5u^4) - s^8(5t^3 + 4t^2u - tu^2 + 4u^3) \\
& + s^2t^3u^3(t^3 + t^2u + 5tu^2 + u^3) - 2(t - u)s^9t]M^2
\end{aligned} \tag{A16}$$

$\gamma_L^* + g \rightarrow c\bar{c}(^3P_J, \frac{1}{2}) + g$: F is the same as Eq.(A12),

$$\begin{aligned}
a = & -Q^2t^2[-8Q^6t^3(s^2 - tu)(st - u^2) - 2Q^4t^2(su(6t^4 + 11t^3u - t^2u^2 + 5tu^3 - u^4) + s^2(t^4 + 9t^3u \\
& + 3t^2u^2 + 5tu^3 - 2u^4) - s^3(5t^3 + 9t^2u + tu^2 + 9u^3) - 2s^4(4t^2 + tu + 3u^2) - 2(t + u)s^5 \\
& + t^4u^2 - 3t^3u^3 - 5t^2u^4 - tu^5) + 2Q^2t(s^2(t^6 + 8t^5u + 11t^4u^2 + 6t^3u^3 + 16t^2u^4 + 4tu^5 + 2u^6) \\
& - s^4(6t^4 + 14t^3u + 11t^2u^2 + 8tu^3 - 7u^4) - s^3u(3t^4 + 14t^3u + 6t^2u^2 + 2tu^3 - 5u^4) + (2t^4
\end{aligned}$$

$$\begin{aligned}
& +8t^3u + 5t^2u^2 + 9tu^3 + 2u^4)stu(t+u) - s^5(8t^3 + 7t^2u + 6tu^2 - 5u^3) - (3t-u)(t+u)s^6 \\
& + t^6u^2 + 2t^5u^3 + t^4u^4) + s(s+u)(s^5(t+u)(3t^2 + u^2) + s^4(9t^4 + 14t^3u + 12t^2u^2 + 2tu^3 + 3u^4) \\
& + s^3(9t^5 + 24t^4u + 32t^3u^2 + 20t^2u^3 + 7tu^4 + 4u^5) + s^2(3t^6 + 18t^5u + 44t^4u^2 + 42t^3u^3 \\
& + 27t^2u^4 + 8tu^5 + 2u^6) + 5st^6u + 25st^5u^2 + 35st^4u^3 + 25st^3u^4 + 12st^2u^5 + 2stu^6 \\
& + 2t^6u^2 + 4t^5u^3 + 2t^4u^4)], \tag{A17}
\end{aligned}$$

$$\begin{aligned}
b = -4(s+t)^2(s+u)t^2M^2Q^2[2Q^2tu(st-u^2) + s(s^2t^2 - s^2u^2 + st^3 - stu^2 - 2su^3 - 2t^2u^2 \\
- 2tu^3 - 2u^4)] \tag{A18}
\end{aligned}$$

$$\begin{aligned}
c = -4Q^2tM^2[-8Q^6t^2(s^2 - tu)(st - u^2) - 2Q^4t(s^2(t^4 + 3t^3u + 4tu^3 - 4u^4) + (2t-u)su(3t^3 \\
+ 5t^2u + 2tu^2 + 2u^3) - (t+2u)s^3(5t^2 - tu + 4u^2) - 4s^4(t^2 + u^2) - 2(t+u)s^5 + t^4u^2 \\
- 5t^3u^3 - 6t^2u^4 - 2tu^5) + 2Q^2(s^2(t^6 + 8t^5u + 9t^4u^2 + 10t^3u^3 + 9t^2u^4 + tu^5 + 2u^6) \\
+ stu(2t^5 + 10t^4u + 11t^3u^2 + 13t^2u^3 + 7tu^4 + u^5) - s^4(t^4 - t^3u - 4t^2u^2 - tu^3 - 6u^4) \\
- s^3u(t+2u)(t^3 - 3t^2u + 2tu^2 - 2u^3) + s^5u(t^2 + tu + 4u^2) + 2s^6u(t+u) + t^6u^2 + 2t^5u^3 \\
- t^3u^5 - t^2u^6) - s(s+u)(3s^5t^2 + 6s^5tu + 3s^5u^2 + 4s^4t^3 + 9s^4t^2u + 10s^4tu^2 + 5s^4u^3 \\
+ 6s^3t^3u + 15s^3t^2u^2 + 14s^3tu^3 + 7s^3u^4 - s^2t^5 + 2s^2t^4u + 12s^2t^3u^2 + 13s^2t^2u^3 + 5s^2tu^4 \\
+ 3s^2u^5 - st^5u - 6st^4u^2 - 6st^3u^3 - 4st^2u^4 + stu^5 + 2su^6 + 4t^3u^4 + 4t^2u^5 + 2tu^6)] \tag{A19}
\end{aligned}$$

$$\begin{aligned}
d = 4Q^2t[4Q^4t^2(st - u^2)(2s^3 - s^2u - 3stu - su^2 - tu^2) + 2Q^2t((2t^4 + 8t^3u + t^2u^2 + 4tu^3 \\
+ u^4)s^2u - s^4(5t^3 + 7t^2u + 4u^3) + s^3u(4t^3 + 5t^2u + 6tu^2 + u^3) - stu^2(t^3 + 2t^2u + 6tu^2 + u^3) \\
- s^5(7t^2 + 3tu + 4u^2) - 2s^6(t+u) - t^4u^3 - t^3u^4 - 2t^2u^5) + s(s+u)(s^5(3t^2 + 2tu - u^2) \\
+ s^4(6t^3 + 4t^2u + 4tu^2 - 2u^3) + s^3(t^4 + 2t^2u^2 - 3u^4) - s^2(4t^5 + 12t^4u + 12t^3u^2 + 14t^2u^3 \\
+ 8tu^4 + 2u^5) - 2st^6 - 12st^5u - 21st^4u^2 - 24st^3u^3 - 19st^2u^4 - 6stu^5 - 2t^6u - 4t^5u^2 \\
- 8t^4u^3 - 6t^3u^4 - 4t^2u^5)] \tag{A19}
\end{aligned}$$

$$\gamma_T^* + q \rightarrow c\bar{c}(^3S_1, \underline{8}) + q: \tag{A20}$$

$$F = \frac{(4\pi)^3 \alpha \alpha_s^2 e_q^2 \langle \mathcal{O}_8^\psi(^3S_1) \rangle}{9(Q^2 - s)^2(Q^2 - u)^2 M^3 s^2}, \tag{A20}$$

$$a = (Q^2t + su)\{2Q^4(s+t)^2 - 2Q^2s[(2t+s)(s+t+u) - tu] + s^2[(s+t)^2 + (t+u)^2]\}, \tag{A21}$$

$$b = 4s^2(Q^2 - u)[Q^2(s+t) - sM^2], \tag{A22}$$

$$\begin{aligned}
c = 4[-2Q^8t + 2Q^6(s^2 + 3st + t^2 + tu) - 4Q^4st(t+u+s) + Q^2s^2(2t^2 - u^2 - s^2 - 4su) \\
+ 2(t+u)s^3u + 2s^4u], \tag{A23}
\end{aligned}$$

$$d = 8s^2(Q^2 - u)(Q^4 + Q^2t - sM^2), \tag{A24}$$

where e_q is the electric charge of the light quark q .

$\gamma_L^* + q \rightarrow c\bar{c}(^3S_1, \underline{8}) + q$: F is the same as Eq.(A20) and $b = 0, d = 0$,

$$a = 2Q^2t(s+t)^2(Q^2-s)^2, \quad (\text{A25})$$

$$c = 8Q^2tM^2(Q^2-s)^2. \quad (\text{A26})$$

$\gamma_T^* + q \rightarrow c\bar{c}(^1S_0, \underline{8}) + q$: $b = c = d = 0$

$$Fa = \frac{4(4\pi)^3\alpha\alpha_s^2e_c^2\langle\mathcal{O}_8^\psi(^1S_0)\rangle}{9s^2Mt(s+u)^2}[2Q^4t^2 + 2Q^2st(s+u) + s^4 + s^2u^2]. \quad (\text{A27})$$

$\gamma_L^* + q \rightarrow c\bar{c}(^1S_0, \underline{8}) + q$: $b = c = d = 0$

$$Fa = \frac{8(4\pi)^3\alpha\alpha_s^2e_c^2\langle\mathcal{O}_8^\psi(^1S_0)\rangle}{9s^2M(s+u)^2}Q^2(Q^2t + su). \quad (\text{A28})$$

$\gamma_T^* + q \rightarrow c\bar{c}(^3P_J, \underline{8}) + q$:

$$F = \frac{16(4\pi)^3\alpha\alpha_s^2e_c^2\langle\mathcal{O}_8^\psi(^3P_0)\rangle}{3M^3s^2t^2(s+u)^4} \quad (\text{A29})$$

$$\begin{aligned} a = & t[-8(s^2+t^2)Q^6t + 2Q^4(s^2(5t^2+4tu+2u^2) + 2st^2(2t-u) + 2s^4 + 4s^3t + 4t^4 + 4t^3u \\ & + t^2u^2) + 2Q^2s(su(t-u)(4t+3u) - s^3(3t+5u) + tu(2t+u)^2 - s^2u(t+5u) - 3s^4) \\ & + s^2(u^2(4t^2+6tu+3u^2) + 2su(4t+5u)(t+u) + 2s^3(3t+5u) \\ & + 2s^2(t+u)(2t+7u) + 3s^4)] \end{aligned} \quad (\text{A30})$$

$$b = -8M^2[Q^2t(s^2(3t+u) + st(t+u) + s^3 + t^2u) - s^2(s+u)((s+t)^2 + tu)] \quad (\text{A31})$$

$$\begin{aligned} c = & 8M^2[-4Q^6t^2 + 2Q^4t((s-t)^2 + (t+u)^2) + Q^2t(4tsu - (s+u)(s-u)^2) \\ & + s^2(u+s+2t)(u+s)^2] \end{aligned} \quad (\text{A32})$$

$$\begin{aligned} d = & 8M^2[-2Q^4t^2(3s+u) + Q^2t(su(4t+u) - 2(t-u)s^2 + s^3 + 2tu^2) \\ & + s^2(s+u)(2s(u+s) + t(u+3s))] \end{aligned} \quad (\text{A33})$$

$\gamma_L^* + q \rightarrow c\bar{c}(^3P_J, \underline{8}) + q$: F is the same as Eq.(A29)

$$\begin{aligned} a = & 2Q^2t^2[-4Q^4t^2 + Q^2t(2s(2t-u) - 3s^2 + (2t+u)^2) \\ & + s(s+u)(4st + su + (2t+u)^2)] \end{aligned} \quad (\text{A34})$$

$$b = -8Q^2t^2M^2(s+u)(s+t) \quad (\text{A35})$$

$$c = 8Q^2tM^2[-4Q^4t + 2Q^2((s-t)^2 + (t+u)^2) - (s+u)((s-u)^2 - 4st)] \quad (\text{A36})$$

$$d = -8Q^2tM^2[2Q^2t(3s+u) - (s+2t)(s+u)^2] \quad (\text{A37})$$

REFERENCES

- [1] M.B. Einhorn and S.D. Ellis, Phys. Rev. **D12**, 2007 (1975); S.D. Ellis et al., Phys. Rev. Lett. **36**; 1263 (1976); C.-H. Chang, Nucl. Phys. **B172**, 425 (1980); E.L. Berger, D. Jones, Phys. Rev. **D23**, 1521 (1981); R. Baier, R. Rückl, Nucl. Phys. **B201**, 1 (1982);
- [2] CDF collaboration, F. Abe *et al.*, Phys. Rev. Lett. **69**, 3704 (1992); Phys. Rev. Lett. **71**, 2537 (1993); Phys. Rev. Lett. **79**, 572 (1997); Phys. Rev. Lett. **79**, 578 (1997)
- [3] G.T. Bodwin, L. Braaten, and G. P. Lepage, Phys. Rev. D51 1125 (1995).
- [4] E. Braaten and S. Fleming, Phys. Rev. Lett. **74**, 3327 (1995); M. Cacciari, M. Greco, M.L. Mangano and A. Petrelli, Phys. Lett. **B356** 553 (1995).
- [5] P. Cho and K. Leibovich, Phys. Rev. D53, 150 (1996); *ibid*, D53, 6203 (1996).
- [6] J. Amundson, *et al.*, Phys. Lett. **B390**, 323 (1997); and references therein.
- [7] P. Hoyer and S. Peigne, Phys. Rev. **D59**, 034011 (1999); N. Marchal, P. Hoyer, and S. Peigne, hep-ph/0004234.
- [8] H1 Collab., S. Aid *et al*, Nucl. Phys. **B472**, 3 (1996).
- [9] ZEUS Collab., M. Derrick *et al*, Eur. Phys. J. **C10**, 373 (1999).
- [10] M. Cacciari and M. Krämer, Phys. Rev. Lett. **76**, 4128 (1996); P. Ko, J. Lee and H.S. Song, Phys. Rev. **D54**, 4312 (1996); J. Amundson, S. Fleming and I. Maksymyk, Phys. Rev. **D56**, 5844 (1997).
- [11] M. Krämer, Nucl. Phys. **B459**, 3 (1996).
- [12] B. Cano-Coloma and M.A. Sanchis-Lozano, Nucl. Phys. **B508**, 75 3 (1997).
- [13] B.A. Kniehl and G. Kramer, Eur. Phys. J. **C6**, 493 (1999).
- [14] M. Beneke I.Z. Rothstein and M. Wise, Phys. Lett. **B408**, 373 (1997); M. Beneke, G.A. Shuler, and S. Wolf, hep-ph/0001062.
- [15] K. Sridhar, A.D. Martin and S.J. Stirling, hep-ph/9806253.
- [16] CDF collaboration, T. Affolder *et al.*, Phys. Rev. Lett. **85**, 2886; CDF Note 4876, 5027, 5029.
- [17] P. Cho and M. Wise, Phys. Lett. **B346**, 129 (1995); M. Beneke and M. Krämer, Phys. Rev. **D 55**, 5269 (1997).
- [18] E. Braaten, B.A. Kniehl, and J. Lee, hep-ph/9911436.
- [19] M. Beneke, M. Krämer and M. Vänttinen, Phys. Rev. **D57**, 4258 (1998).
- [20] S. Fleming and T. Mehen, Phys. Rev. **D57**, 1846 (1998).
- [21] P. De Causmaecker, R. Gastmans, W. Troost, T.T. Wu, Phys. Lett. **B 105**, 215 (1981), Nucl. Phys. **B206**, 53 (1982); R. Gastmans, W. Troost, T.T. Wu, Nucl. Phys. **B291**, 731 (1987).
- [22] H. Merabet, J.-F. Mathiot, and R. Mendez-Galain, Z. Phys. **C62**, 639 (1994).
- [23] J.Ph. Guillet, Z. Phys. **C39**, 75 (1988).
- [24] M. Glück, E. Reya and A. Vogt, Z. Phys. **C67**, 433 (1995).
- [25] M. Beneke and M. Krämer, Phys. Rev. **D 55**, 5269 (1997).
- [26] J.K. Mizukoshi, hep-ph/9911384.
- [27] B. A. Kniehl and L. Zwirner, [arXiv:hep-ph/0112199].

Figure Captions

FIG. 1. The differential cross section $d\sigma/dz$ as a function of z for J/ψ production in DIS at HERA: $2GeV^2 < Q^2 < 80GeV^2$, $40GeV < W_{\gamma^*p} < 180GeV$. The dotted line is for the color-singlet contributions, the dotted-dashed line for the direct virtual photon contributions from the color-octet processes, and the dashed line for the resolved virtual photon contributions from the color-octet processes, where octet matrix elements take values as $\langle \mathcal{O}_8^\psi(1S_0) \rangle = \langle \mathcal{O}_8^\psi(3P_0) \rangle / m_c^2 = 0.008GeV^3$. The solid lines correspond to the total cross sections for the two choices of the color-octet matrix elements: (I) the lower solid line for choice of Eq. (23), and (II) the upper solid line for Eq. (24).

FIG. 2. The polarization parameter α as a function of z in γ^*p processes, where $W_{\gamma^*p} = 100GeV$ with four typical values for Q^2 . The solid lines are for the CSM predictions, and the other two lines are for the NRQCD FA predictions (including both the color-singlet and color-octet contributions): the dashed lines for the choice of Eq. (23) and the dotted-dashed lines for the choice of Eq. (24).

FIG. 3. α as a function of z for J/ψ production in DIS at HERA. The definitions of the curves are the same as those of Fig. 2.

FIG. 4. The same as the plot of Fig. 3, but with different parameterizations for the color-octet matrix elements (here Eqs. (25) and (26) are used). The solid lines is the CSM prediction, and the other two lines are for the NRQCD FA predictions: the dashed line for the parameterization of Eq. (25) and the dotted-dashed line for the parameterization of Eq. (26).

FIGURES

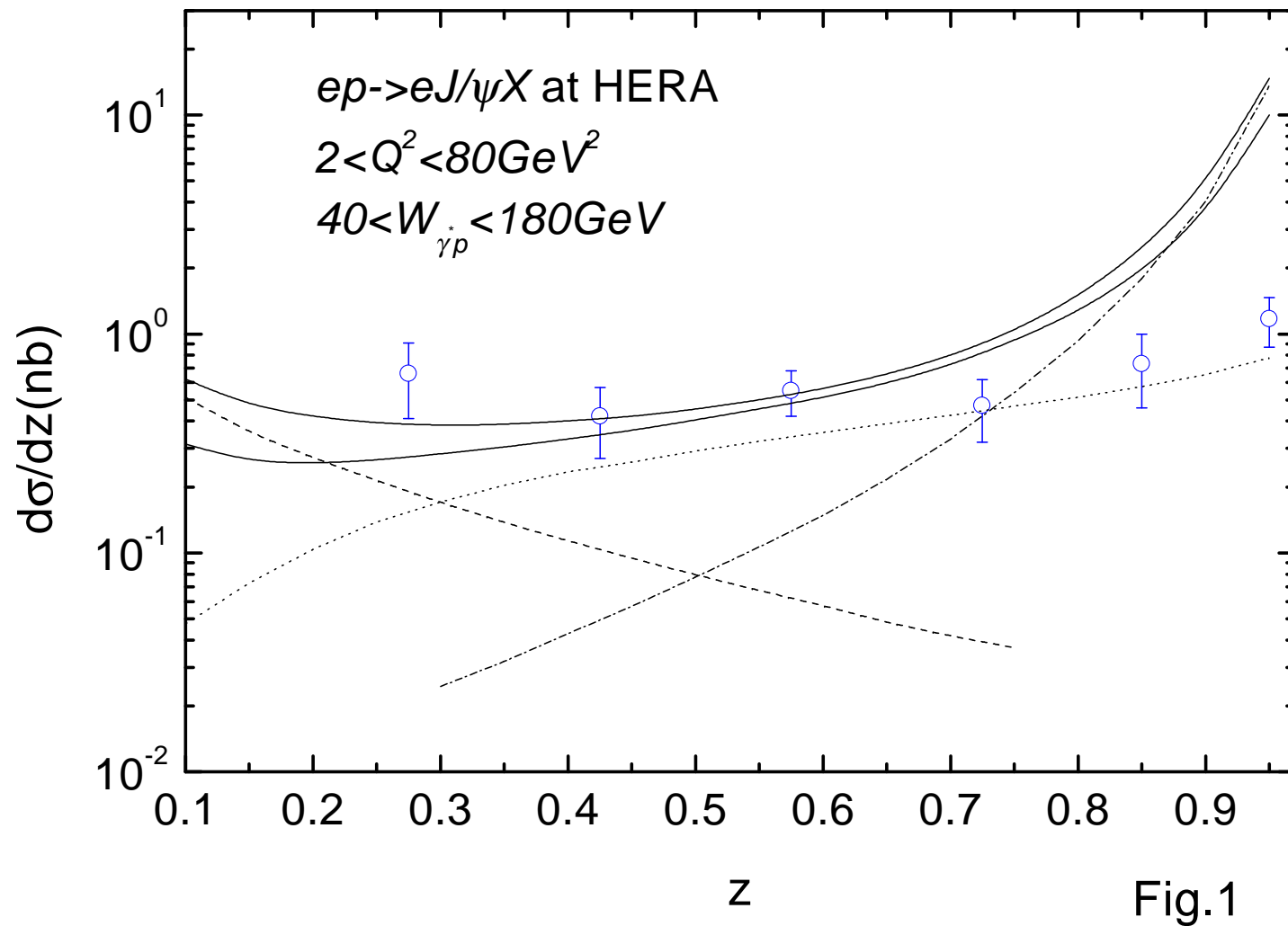


Fig.1

$\gamma^* p$ collisions, $E_{\gamma^* p} = 100 \text{ GeV}$

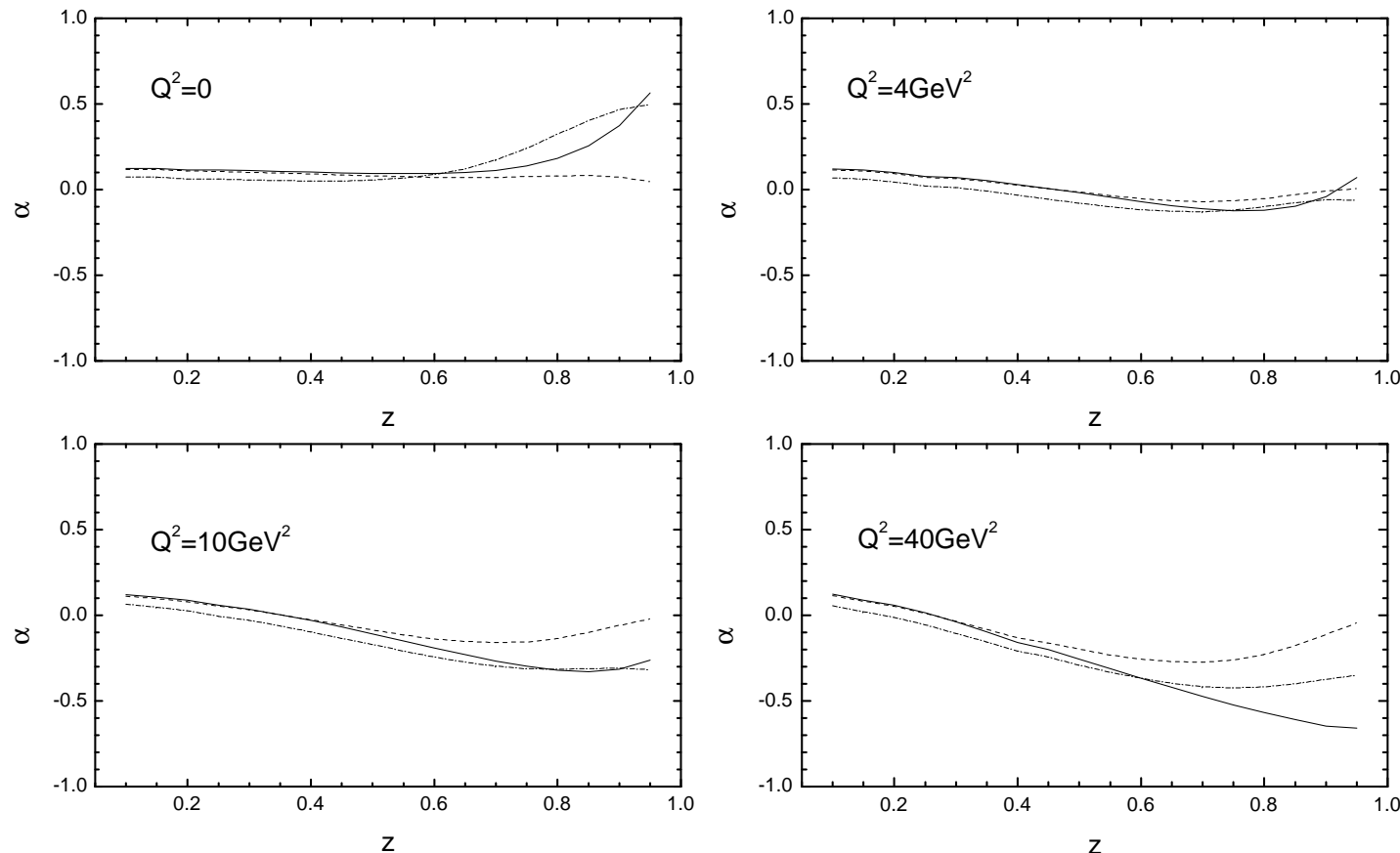


Fig.2

ep collisions ($E_{ep} = 300\text{GeV}$, $40\text{GeV} < W_{\gamma p} < 180\text{GeV}$)

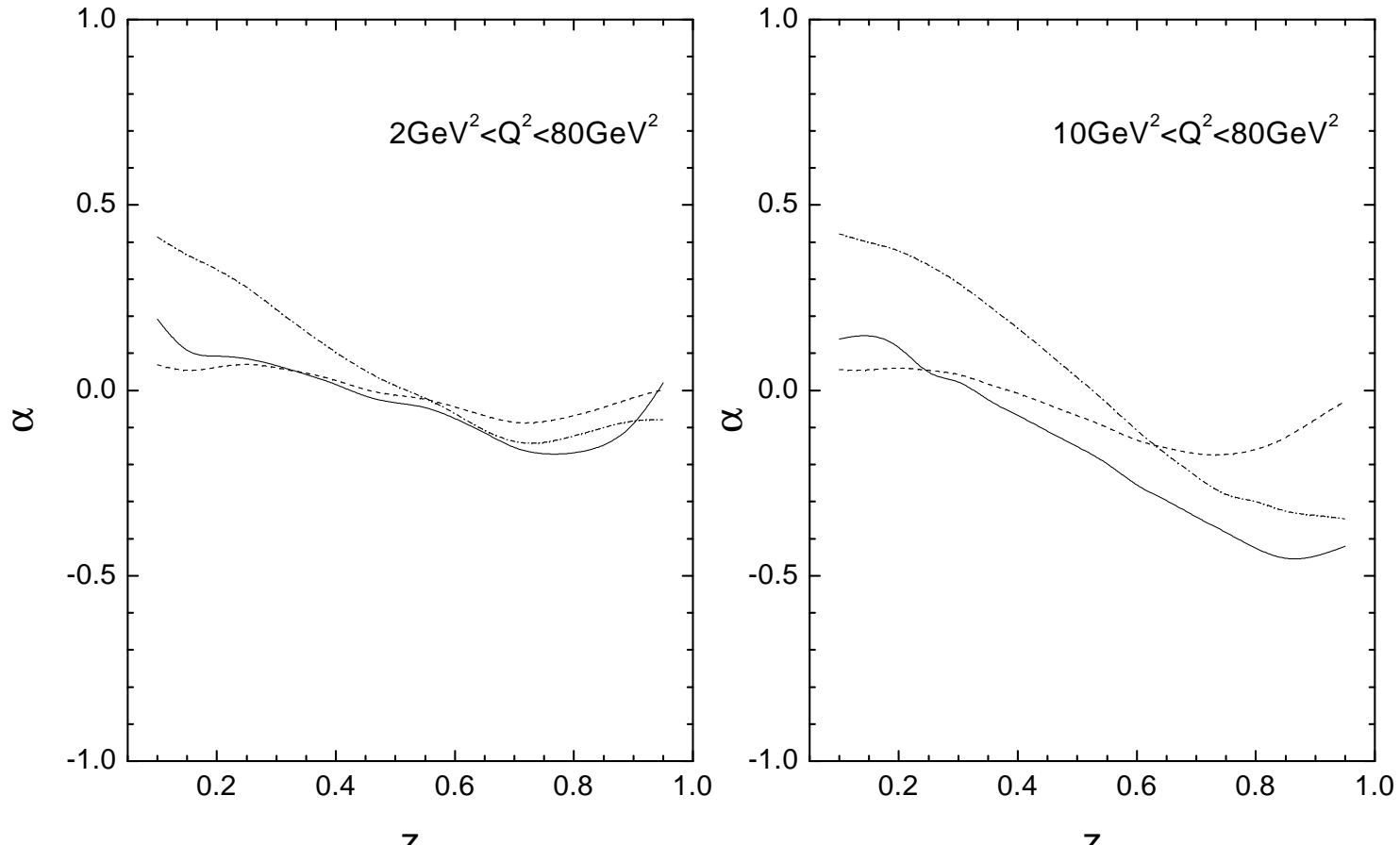


Fig.3

$10\text{GeV}^2 < Q^2 < 80\text{GeV}^2$

